Int. J. Heat Mass Transfer. Vol. 27, No. 3, pp. 363–374, 1984
Printed in Great Britain

0017 9310/84 $3.00+0.00

STUDY OF LIQUID SPRAY (WATER) IN A CONDENSABLE ENVIRONMENT (STEAM)

S. Y. LEE* and R. S. TANKIN
Department of Mechanical and Nuclear Engineering, Northwestern University, Evanston, IL 60201, U.S.A.

(*Received* 29 *June* 1982 *and in revised form* 13 *June* 1983)

Abstract—A model to describe the behavior of a subcooled water spray in a steam environment is proposed. The pressure drop within the sheet portion of the spray is due to condensation. This pressure drop is sufficient to cause the sheet portion to contract, and to reduce the spray angle. Computed results were compared with experiments and agreement is reasonable. In these experiments the fluid flow in sheet portion, based on Reynolds number, is laminar. This is also assumed in the computations since molecular conductivity values were used for calculating the heat transfer in the subcooled water. A correlation of breakup length with Weber and Jakob numbers was obtained.

NOMENCLATURE

a	distribution parameter
A_0	flow area of the nozzle [m^2]
C_D	drag coefficient
C_p	specific heat of liquid [$kJ\ kg^{-1}\ K^{-1}$]
D	diameter of droplets [μm]
D_i	initial droplet diameter [μm]
D_m	maximum droplet diameter [μm]
D_n	nozzle orifice (hydraulic) diameter
Fo	Fourier number ($4\alpha\theta/D_i^2$)
g	gravity
h	enthalpy [$kJ\ kg^{-1}$]
Ja	Jacob number, $C_p(T_s-T)/\lambda$
L	length of liquid spray sheet [m]
$\dot{m}_{c,z}$	condensation rate between $z-z+dz$ [$kg\ s^{-1}$]
n	normal to the flow direction
N	number of droplets
P	pressure of vapor [$N\ m^{-2}$]
Q	volume flow rate of liquid [$ml\ s^{-1}$]
r	radial distance from the axis [m]
R	radius of spray cross section at z [m]
S	direction of liquid flow
t	thickness of liquid sheet [m]
T	temperature [°C]
T_{L0}	temperature of spray liquid at the nozzle exit [°C]
T_i	temperature of liquid droplet at breakup point [°C]
T_s	temperature of steam [°C]
V_{L0}	liquid velocity of the sheet portion [$m\ s^{-1}$]
$V_{L,z}$	liquid velocity (axial direction) [$m\ s^{-1}$]
V_0	velocity difference between liquid and steam (or air)
$V_{v,z}$	steam (or air) velocity (axial direction) [$m\ s^{-1}$]
$V_{v,r}$	steam (or air) velocity (radial direction) [$m\ s^{-1}$]
V_t	tangential velocity of liquid [$m\ s^{-1}$]
We	Weber number, $\rho_L V_{L0}^2 D_n/\sigma$
y	$\ln[\bar{a}D/(D_m-D)]$
z	axial distance from the nozzle tip [m].

Greek symbols

α	thermal diffusivity [$m^2\ s^{-1}$] $[1+C_p(T_s-T_i)/\lambda]^{1/3}-1$
δ	distribution parameter
ζ	radius of curvature
θ	time [s]
λ	heat of vaporization [$kJ\ kg^{-1}$]
ρ_L	liquid density [$kg\ m^{-3}$]
ρ_v	vapor density [$kg\ m^{-3}$]
σ	surface tension [$N\ m^{-1}$]
ϕ	$\tan^{-1}(dr/dz)$.

1. INTRODUCTION

THE MANUFACTURERS of spray nozzles provide data concerning the operating ranges for their nozzles, spray angles, general information about droplet sizes, and statements concerning droplet distributions (full cone, hollow cone, etc.). This information is restricted to nozzles that operate in a quiescent non-condensable (air) environment. (A water spray in an air environment has been discussed in ref. [1], which is designated as Paper I). In many cases, this information is sufficient for selecting an appropriate nozzle for the task under consideration. However, there are situations where this information is not adequate. For example, the spray angle is often known to contract when a subcooled liquid is sprayed into a condensable environment.

There are many examples of sprays in a condensable environment; for example, subcooled water is sprayed into steam in a direct contact condenser; a cold water spray is injected into steam when a LOCA situation occurs in a nuclear reactor, etc. Although this problem

* Present address: Department of Mechanical Engineering, Korea Advanced Institute of Science and Technology, Seoul, Korea.

exists in many engineering applications, only limited research has been conducted on sprays in a condensable environment. There have been condensation studies conducted on droplets, jets, and stratified flow. For instance, Brown [2, 3] studied the effects of mean droplet diameter and water feed rate on heat transfer for water droplets in a steam environment. Lim *et al.* [4] determined the heat transfer coefficient in the case of stratified steam–water flow; laminar liquid jet heat transfer rates were determined for a water jet in a steam environment by Hasson *et al.* [5, 6]. Kutateladze [7] made calculations for turbulent heat transfer rates for a free falling jet.

Weinberg [8] studied the heat transfer for sprays of water in a steam environment at low pressures. He divided the spray into two regions—sheet region and droplet region, and concluded that most of the heat transfer takes place in the sheet region. Lekic and co-workers [9–11] studied the behavior of droplets experimentally and devised an analytical model of the spray. Drop size distributions were measured and the theoretical considerations included the motion of droplets (vertical direction only) and heat transfer rate. In this analysis, the thermal utilization for a given length of spray is obtained. More recently, a water spray in a steam environment was studied by Sandoz and co-workers [12, 13] and the General Electric Company [14] for LOCA situations in a nuclear reactor. They studied modeling of environmental effects on the water sprays from nozzles used in reactors. These studies did not contain a detailed examination of the spray, i.e. sheet region, drop size distribution, breakup lengths, etc. but concentrated on the prototype equipment for design purposes.

The present research is an extension of the work presented in Paper I to include condensation effects. When relevant, a comparison is made between sprays in steam and in air. Most of the equations and experimental techniques used in this study, with suitable modifications, were presented in Paper I.

2. ANALYTICAL MODEL

2.1. *Introduction*

Usually the nozzles used in direct contact condensation are wide angle nozzles and are classified as hollow cone nozzles. We will confine our attention to hollow cone sprays—generated by either a swirl nozzle or a poppet type nozzle. In Paper I, we limited our analysis to a poppet type nozzle although swirl nozzles were also studied and agreement existed between experiments and computed curves for spray angles.

2.2. *Sheet region of spray*

As in the non-condensable case, the spray may be divided into three regions: sheet region, breakup region and droplet region. For the sheet region, the following assumptions will be made:

(1) Condensation has a negligible effect on the liquid sheet thickness (the mass flow rate of the vapor is small compared to the mass flow rate of the liquid).

(2) The effect of friction drag on the liquid sheet is neglected.

(3) Pressure of the vapor inside the sheet portion is a function of axial distance (z) only.

(4) Gravity force is negligible.

(5) Velocity of the vapor inside the sheet portion (away from the sheet boundary) is a function of axial distance (z) only.

For the non-condensable case, the circulation pattern within the sheet region consists of closed streamlines (see Fig. 1). This has been discussed in detail in Paper I. When condensation is present, the flow pattern is assumed to be as shown in Fig. 2. The entrainment of vapor from the surroundings is more vigorous when condensation is present. Small secondary flow is expected at the edge of the sheet region, which enhances the breakup of the sheet. Experimentally it was found that for the same water flow rates, the length of the water sheet is shorter in condensing flows than in non-condensing flows. With

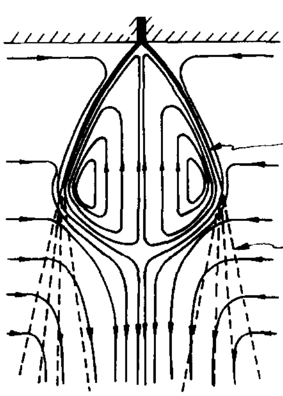

FIG. 1. General flow pattern of spray in the case of no condensation.

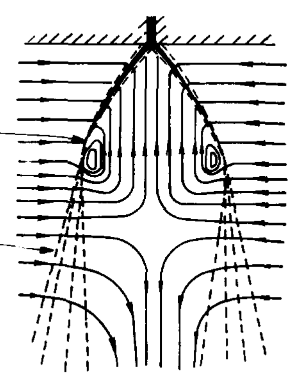

FIG. 2. General flow pattern of spray in the case of condensation.

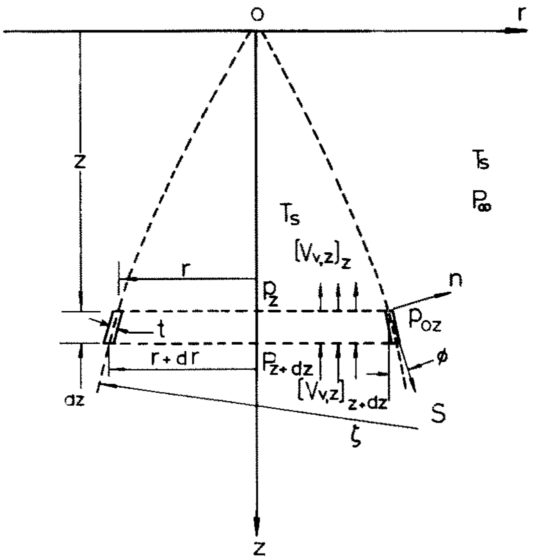

FIG. 3. Diagram showing the coordinate and symbols used in computing the sheet portion of the spray.

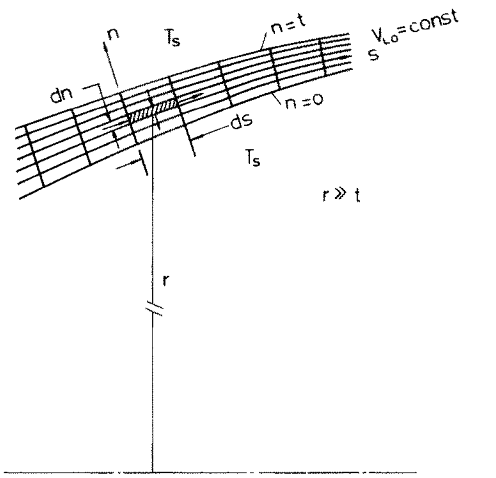

FIG. 4. Coordinate system used for energy balance in the liquid sheet calculation.

these general concepts, an analytical model for the spray with condensation is proposed.

A force balance for the free body diagram shown in Fig. 3 yields

$$\frac{2\sigma}{\zeta}+\frac{2\sigma}{r/\cos\phi}+\Delta P-\frac{V_{\mathrm{LO}}^2\rho_{\mathrm{L}}t}{\zeta}-\frac{V_t^2\rho_{\mathrm{L}}t}{r/\cos\phi}=0, \quad (1)$$

where ζ is the radius of curvature. These terms are described in Paper I except for the fifth term which is a centrifugal force due to the swirl of the spray (not present for the poppet nozzle). With no frictional drag

$$V_{\mathrm{LO}}=\text{const.} \quad (2)$$

and

$$V_t r=\text{const.} \quad (3)$$

With condensation, the heat transfer coefficient at the steam–water interface is very high (about 100 kW $\mathrm{m}^{-2}\ \mathrm{K}^{-1}$, refs. [5, 6]). Thus, it is assumed there is no heat transfer resistance on the vapor side of the interface; the entire resistance occurs on the liquid side. The removal of heat from the interface is assumed to be by conduction in the liquid. Assuming molecular conductivity limits the analysis to laminar flow in the sheet region. Thus, the energy balance equation is

$$V_{\mathrm{LO}}\frac{\partial T}{\partial S}=\alpha\frac{\partial^2 T}{\partial n^2}, \quad (4)$$

with boundary conditions

$$T(S,0)=T_s,\qquad T(S,t)=T_s,\qquad T(0,n)=T_{\mathrm{LO}}, \quad (5)$$

where S is in the direction of the liquid flow and n is normal to the flow direction (Fig. 4). With V_{LO} assumed to be constant, equation (4) can be rewritten as

$$\frac{\partial T}{\partial\theta}=\alpha\frac{\partial^2 T}{\partial n^2}, \quad (6)$$

where θ is time. The boundary conditions are

$$T(\theta,0)=T_s,\qquad T(\theta,t)=T_s,\qquad T(0,n)=T_{\mathrm{LO}}. \quad (7)$$

This is a classic problem in transient conduction heat transfer. It should be mentioned that the water sheet thickness, t, and the distances between streamlines, $\mathrm{d}n$, are changing as S increases. Therefore, the solution of equations (6) and (7) can be obtained numerically. If the water sheet thickness is given as a function of S (or θ), the analytical solution can be obtained by coordinate transformation.

For the test facilities used in this experiment, the liquid flow is limited by the rate at which steam can be generated. For these conditions, the flow in the liquid sheet is laminar. In the future, experiments will be conducted using the building steam supply which will allow us to operate in the turbulent regime.

The temperature distribution in each segment can be obtained from the solution of equation (6) and thus the enthalpy flux for each segment can be computed

$$h_z=\int_0^t\left\{\rho_{\mathrm{L}}C_pT2\pi r\sqrt{\left[1+\left(\frac{\mathrm{d}r}{\mathrm{d}z}\right)^2\right]}\mathrm{d}z\right\}\mathrm{d}n. \quad (8)$$

From an energy balance, the condensation rate for each segment can be determined

$$\lambda\dot{m}_{c,z}=\frac{\mathrm{d}}{\mathrm{d}\theta}(h_z). \quad (9)$$

Since there is no heat transfer resistance on the vapor side of the interface and heat is removed from the interface by conduction in the liquid, half of the condensation occurs inside the sheet segment (half on the outside). Thus for the inner surface

$$\int_0^z \frac{1}{2}\frac{\dot{m}_{c,z}}{dz}\,dz = \rho_v(\pi r^2)(V_{v,z}). \quad (10)$$

The pressure difference between the inside and outside of the sheet for each segment is

$$\Delta P = \tfrac{1}{2}\rho_v V_{v,z}^2. \quad (11)$$

The pressure drop due to flow of vapor through the breakup region (past the droplets) is assumed to be negligible. From the equations presented, the radius of the water sheet can be computed numerically. The point to be noted, is that the shape of the sheet is computed without any adjustable coefficients!

2.3. *Droplet portion of the spray*

As stated in Paper I, entrainment of the vapor will drag the droplets inwards. Similar assumptions as listed in Paper I are assumed in this analysis with regard to the droplet; such as, droplets are spherical, upper-limit drop size distribution function applies, vapor pressure equals ambient pressure, no droplet interaction, initial velocity and initial temperature of droplets obtained from sheet portion computation at breakup point, etc. The droplet size is changed by condensation [9]; that is

$$D = D_i\{1+\Gamma(1-\exp(-\pi^2 Fo))^{1/2}\},$$

where

$$\Gamma = \left[1+\frac{C_p(T_s-T_i)}{\lambda}\right]^{1/3} - 1, \quad (12)$$

$$Fo = \frac{4\alpha\theta}{D_i^2}.$$

Equation (12) is obtained neglecting thermal resistance in the vapor and neglecting internal circulation in the droplet. Kashiwagi and Oketani [15] substantiates the resistance in the vapor is negligible for droplets of subcooled water in steam. Ohba *et al.* [16] examined the effects of internal circulation. Their analytical results did not agree well with experiments of others. Hence the assumption was made that heat transfer for droplets occurs by conduction.

The unbalanced forces on the droplets result in the following equation

$$\left(\frac{\pi}{6}D^3\rho_L\right)\frac{d\mathbf{V}_L}{d\theta} = -(\mathbf{V}_L-\mathbf{V}_v)\frac{d}{d\theta}\left(\frac{\pi}{6}D^3\rho_L\right) - \frac{1}{2}\left(\rho_v C_D \frac{\pi}{4}D^2\right)V_0(\mathbf{V}_L-\mathbf{V}_v) \quad (13)$$

where

$$V_0 = |\mathbf{V}_L - \mathbf{V}_v|.$$

The z directional momentum balance is

$$\underbrace{\int_{D_i}\frac{\pi}{6}D^3\rho_L V_{L,z}\,dN_i}_{\text{momentum of droplets}} + \underbrace{\int_R 2\pi r\rho_v V_{v,z}^2\,dr}_{\text{momentum of vapor}} = \text{const.} \quad (14)$$

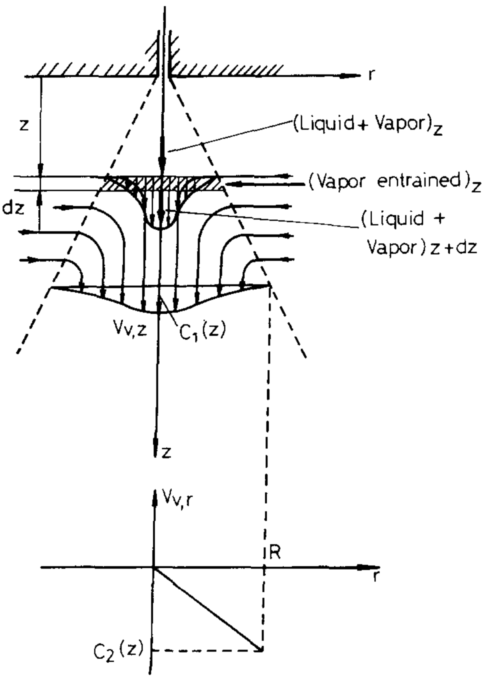

FIG. 5. Vapor velocity profile used in the droplet portion of the spray.

The mathematical expressions used for the vapor velocity (see Fig. 5) were discussed in Paper I.

The mass flux of the liquid and vapor are balanced as

$$2\pi R V_{v,r}\rho_v\,dz = \int_0^{R+dR} 2\pi r\rho_v[V_{v,z}]_{z+dz}\,dr - \int_0^R 2\pi r\rho_v[V_{v,z}]_z\,dr + \frac{\pi}{6}\rho_L\int_{D_i}(D_{z+dz}^3 - D_z^3)\,dN_i. \quad (15)$$

The velocity and positions of droplets are computed for each segment of the spray in a manner similar to that described in Paper I. From these velocities and positions, the trajectories of the droplets are computed.

3. EXPERIMENTS

A schematic diagram of the system is shown in Fig. 5 of Paper I. Figure 6 is a drawing of the test chamber. Steam is generated by boiling water with an electric heater that is located in the bottom of the test chamber. The steam which is generated in the test chamber is maintained at the desired pressure by means of a relief valve. Water is supplied to the nozzle at a pre-selected flow rate and temperature. Experiments were conducted at various water flow rates (2.23–9.4 ml s^{-1}) various temperatures (20°C to saturation temperature), and various pressures (1–3 atm).

The test chamber is made of brass—25 cm in diameter, 30 cm high—and contains windows (5 cm in diameter) for taking photographs and holograms. To eliminate condensation on windows, electric heating

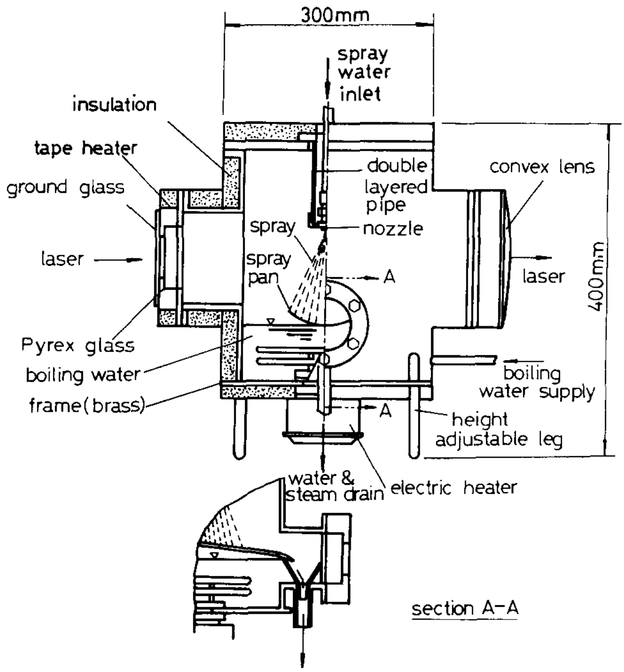

FIG. 6. Sketch of the test section.

tapes are used to maintain the windows at a temperature slightly above the saturation temperature. A spray pan is located inside the test chamber to deflect the spray water; thus minimizing the mixing of the spray water with the boiling water. The spray nozzles used are both swirl ($\frac{1}{4}$TTGO.3 and $\frac{1}{4}$TTGO.4 manufactured by Spraying Systems Co., Wheaton, Illinois) and poppet nozzles. Details are presented in Table 1.

Before water is supplied to the nozzle, the water inside the test chamber is boiled for at least 1 h—exhausting steam from the test chamber—thus eliminating all air from the test chamber. Water is then supplied to the nozzle at a pre-selected temperature (by heating tape on the water supply pipe) and flow rate. Steam is continuously exhausted from the test section during the experiments to reduce the possibility of the build up of non-condensables from the water. When steady-state conditions are obtained (from thermocouple and pressure readings in the test chamber) holograms or normal photographs are taken.

4. RESULTS AND DISCUSSION

4.1. *Sheet portion of the spray*

Two major quantities for the sheet portion are determined from the holograms and photographs—spray angle and breakup length. Experiments were performed on four nozzles (Nos. 1–4) in both air and steam. Figure 7 shows typical photographs of these sprays—air and steam environments are compared. In Fig. 8 typical traces of the sheet portion are shown for Nozzle 2 (swirl nozzle). Each rippled line is an outline of

Table 1. Specification of the nozzles used in experiments

Nozzle	Type	Specifications
1	Spraying Systems, Type TG Full Cone Spray Nozzle, $\frac{1}{4}$ TTGO.3	D_n(Orifice diameter) = 0.02 in. (0.508 mm) with two slots for swirling inside the nozzle
2	Spraying Systems, Type TG Full Cone Spray Nozzle, $\frac{1}{4}$ TTGO.4	D_n(Orifice diameter) = 0.023 in.* (0.584 mm) with two slots for swirling inside the nozzle
3	Poppet type nozzle	Equivalent diameter of orifice = 0.406 mm Flow area = 0.858 mm^2
4	Poppet type nozzle	Equivalent diameter of orifice = 0.445 mm Flow area = 0.439 mm^2

* Original specification in the catalogue shows 0.022 in. However, the measured size is 0.023 in. (measured with an optical comparator).

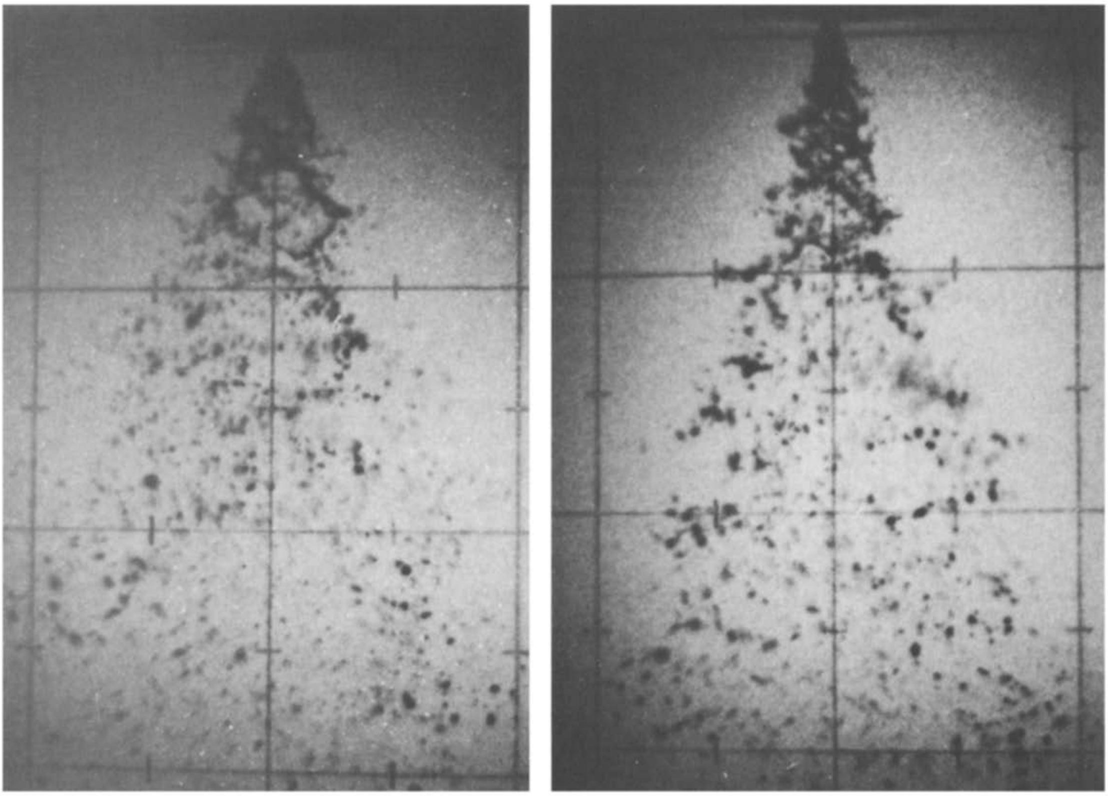

FIG. 7. Typical photographs of the spray (Nozzle 2).

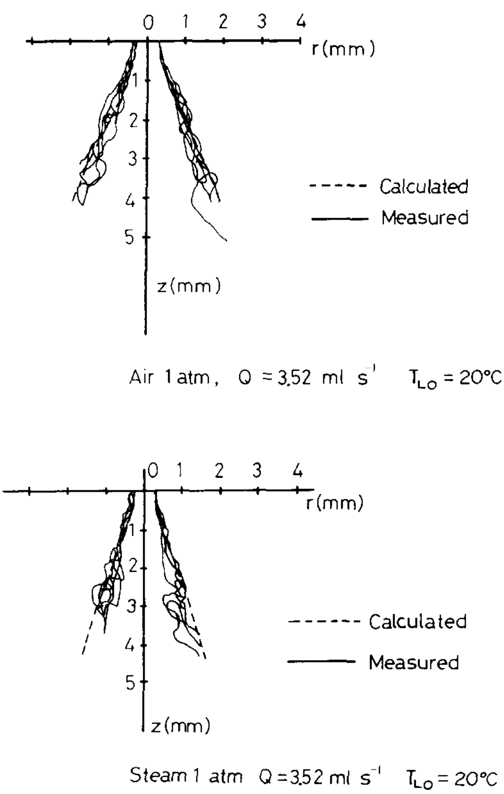

FIG. 8. Calculated and measured shape of sheet portion (Nozzle 2, $V_t/V_{LO} = 0.45$ at nozzle exit).

the shape of the sheet portion traced from a photograph (such as Fig. 7). Five or six photographs were taken for each set of conditions. In these figures the computed sheet profile is shown as a dashed curve. It is seen that the computed profile is in reasonable agreement with the experimental observations. When experimentally time-averaged profiles (obtained by averaging the values from five photographs—such as in Fig. 7) are compared with computed values, the agreement is excellent. For the swirl nozzles the computed shape shows a concave portion near the nozzle. In all cases, the breakup length in air was equal to or greater than the breakup length in steam; in most cases it was significantly greater. Similar results were reported by Sandoz *et al.* [13]. In Sandoz's experiments in a steam environment there is a marked change in the slope in the spray profile at the breakup point for a swirl type nozzle. A possible explanation for the change in the slope is as follows: Assuming a potential, vortex flow, where $V_t r$ = const., contraction of spray angle results in an increase in the tangential velocity. This, in turn, causes a greater centrifugal force which is no longer balanced by pressure and surface tension forces after breakup. One would not expect this abrupt change in shape of profile with a poppet nozzle since no swirl is present. Our experiments bear out this statement.

4.2. *Breakup region of the spray*

In this study 389 photographs for the four different

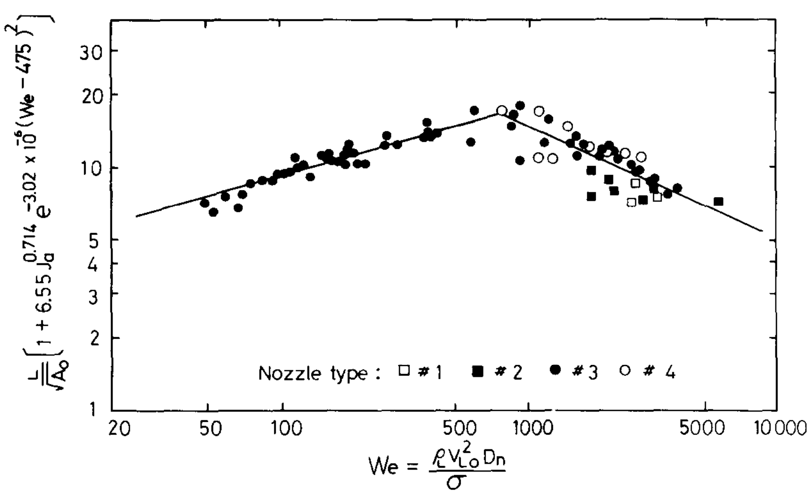

FIG. 9. Breakup length of the liquid sheet as a function of Weber and Jakob numbers.

nozzles (two swirl and two poppet types) were examined to determine if a correlation could be obtained relating breakup length to Weber and Jakob numbers. In these experiments, the Weber number ranged from 30 to 5000 and the initial spray angle between 40° and 60°. The results are plotted in Fig. 9. The following equation was fitted to the experimental data

$$\frac{L}{\sqrt{A_0}}\left[1+C_1(Ja)^{C_2}\,e^{-C_3(We-C_4)^2}\right] = C_5\,We^{C_6}, \quad (16)$$

where

$C_1 = 6.5,$

$C_2 = 0.7,$

$C_3 = 3\times10^{-6},$

$C_4 = 475,$

and

$C_5 = 2.50, \quad (We < 750); \quad C_5 = 350, \quad (We > 750);$

$C_6 = 0.30, \quad (We < 750); \quad C_6 = -0.45, \quad (We > 750).$

The constants were determined from a best-fit curve to the data points by a non-linear, least square method. We are concerned using a best fit involving six constants, but at present there is nothing better to use and the data appears to agree with this best-fit curve. Equation (16) is an improved correlation over that presented in Paper I where only one type of nozzle and a spray in a non-condensable medium was reported. For a poppet type nozzle, the Weber number is based on the hydraulic diameter.

Huang [17] studied the breakup of the liquid sheet formed by impinging two liquid jets from opposite directions. His experiments covered the Weber number range from 100 to 40 000, and showed the peak value of breakup length at a Weber number between 800 and 1000. Huang's definition of non-dimensionalized breakup length differs from ours, and if his results are converted to our scale, his magnitudes are in agreement with ours within a factor of 2. This difference, we think, is due to the radically different methods in creating the sheet. According to Sandoz [18], her experimental results show the breakup length occurs at 5 ~ 10 orifice

Table 2. Parameters of drop size distribution functions of each test condition (Nozzle 1)

Test condition	1	2	3	4	5	6	7
Environment	Air 1 atm		Saturated steam 1 atm			Air 3 atm	Saturated steam 3 atm
Spray water flow rate (ml s^{-1})	3.52	2.23	2.23	3.52	3.52	3.52	3.52
Spray water temperature (°C)	13.0	13.1	24.5	24.5	61.1	15.0	24.5
Saturation temperature (°C)	—	—	100	100	100	—	134.0
a	2.79	1.97	2.44	1.79	1.77	2.03	2.32
δ	1.40	1.17	1.19	1.07	1.33	1.22	1.16
D_m (μm)	972.3	936.0	1320.0	908.8	676.0	688.5	966.5
Drop size distribution function (upper limit function)	$\frac{dv}{dD} = \frac{\delta}{\sqrt{\pi}}\frac{D_m}{D(D_m-D)}\exp(-\delta^2 y^2), \quad y = \ln[aD/(D_m-D)]$						

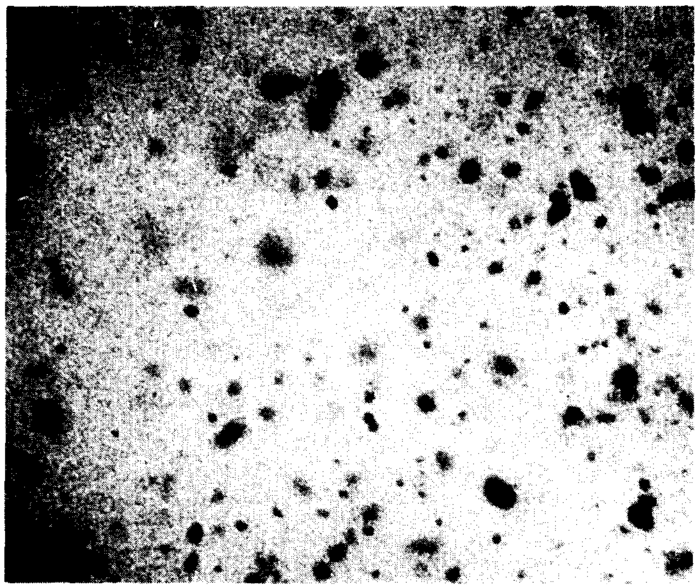

Fig. 10. Typical photograph of spray droplets taken from hologram.

diameters from the nozzle exit. The Weber number range of Sandoz's experiment varies from approximately 10^4 to 10^5, and her results are in agreement with the extrapolation of our data within a factor of 2. Her nozzle flow is probably in the turbulent range whereas ours is laminar. Therefore, the general trend of breakup length is given by equation (16) and should apply within a factor of 2 for nozzles of different shapes, sizes and flow rates.

4.3. *Droplet portion of the spray*

Experiments were conducted for test conditions such as those listed in Table 2 for Nozzle 1. In the region 10–25 mm from the nozzle, the diameters and positions of the droplets are measured from holograms. Figure 10 shows a typical photograph taken from a hologram. Note that some droplets are in focus; whereas, others are out of focus. By traversing the camera other droplets are in focus. In determining droplet size distributions, the droplets are grouped in 50 μm increments. Non-spherical drops are handled as ellipsoids. For test conditions 1–7, the droplet sizes range from 50 to 750 μm. The following conclusions can be drawn about the droplet distributions. The average droplet size is larger in a steam environment than an air environment. This is partly due to condensation of steam on subcooled

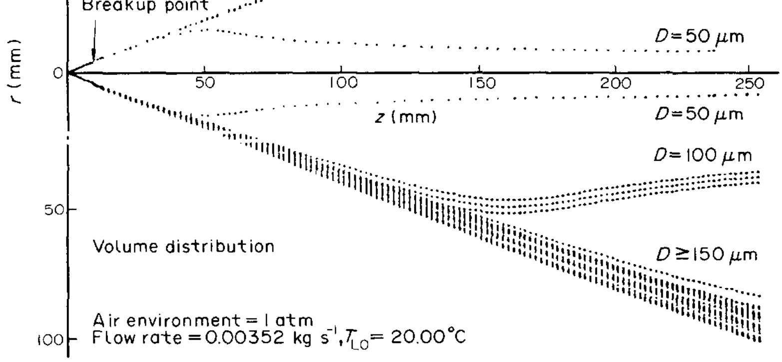

Fig. 11. Shape of typically computed spray showing both sheet and droplet regions (Nozzle 1, air environment).

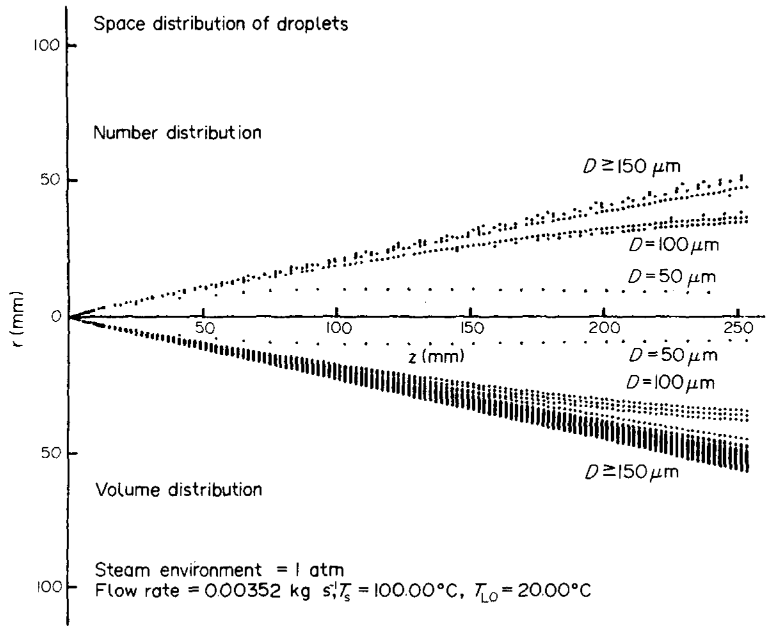

FIG. 12. Shape of typically computed spray showing both sheet and droplet regions (Nozzle 1, 20°C water in steam environment).

water droplets but perhaps and more significantly, due to a shorter breakup length of the water sheet in a steam environment. Droplet sizes become more uniform and smaller when ambient pressure increases (same water flow rates). This coincides with results obtained by other investigators [19–21]. When inlet water temperatures increase, the droplet sizes become smaller, and the distribution curve approximates that of an air environment.

The droplet size distributions were used to compute the droplet trajectories. Figures 11 and 12 show the calculated sprays. For calculation purposes, the drops are grouped in 50 μm increments (as in the experimental measurements). The initial droplet velocities and temperatures are taken as the values computed in the sheet region at the breakup point. From the computations, the smallest droplets are deflected inward significantly, whereas the majority of the droplets are not. In Fig. 12, the sheet portion is contracted due to condensation, and the spray angle is significantly reduced. These computed profiles show the spray angle is primarily determined by the sheet

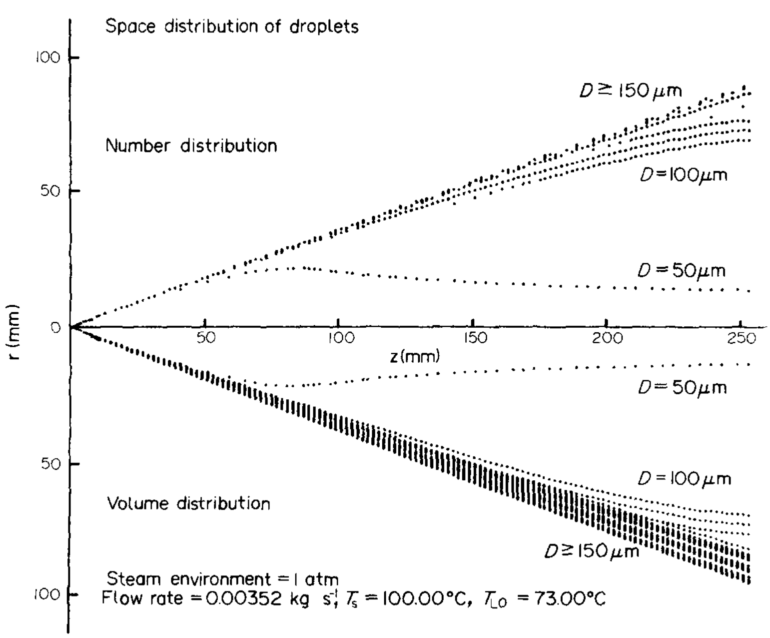

FIG. 13. Shape of typically computed spray showing both sheet and droplet regions (Nozzle 1, 73°C water in steam environment).

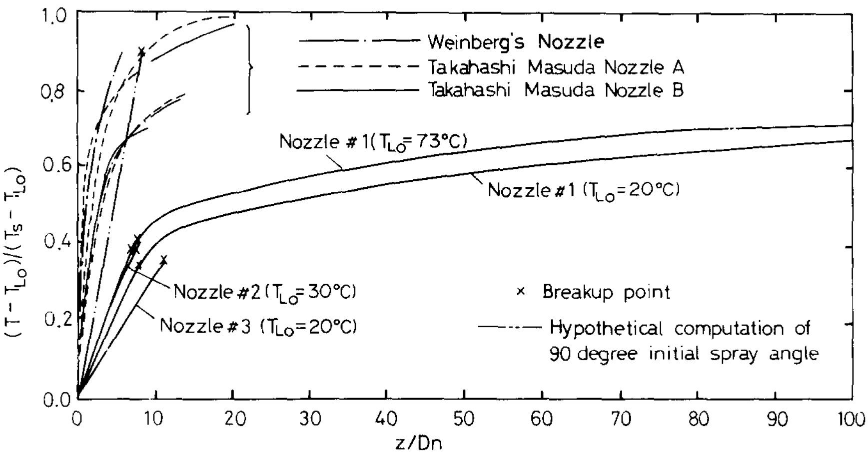

FIG. 14. Temperature variation of water spray along axial direction.

region of the spray, not the droplet region. Similar conclusions are reported by Chan *et al.* [22]. When the inlet temperature of the water spray is closer to the saturation temperature the spray shape is similar to a spray in an air environment. This is seen in Fig. 13 (same water flow rate as in Fig. 12) where the inlet water temperature is 73°C. This is also observed experimentally. The computations reveal that the deflection of the smaller droplets inwards is greater in an air environment than in a steam environment (compare Figs. 11 and 13). The density of air is greater than that of steam; thus for the same entrainment one would expect the drag force to be higher in air than in steam. Another point to be noted is that the computed water temperature at breakup has risen appreciably (see Fig. 14) and thus the condensation contribution to the entrainment is not dominant in the droplet region of the spray. This is evident in Fig. 14 where the temperature of the water spray is plotted vs distance from nozzle. The breakup points are designated by crosses or occur where there is an abrupt change in the slope of the curve.

Weinberg [8] and Takahashi *et al.* [23] measured the spray water temperature and their results are also plotted in Fig. 14. Their curves are much steeper, but their spray angle is much greater—85°–90° compared with ours of 40°–60°. Computations were made for a 90° spray angle using the correlation given in equation (16) to determine the breakup length. These results, also shown in Fig. 14, are in reasonable agreement with Weinberg's and Takahashi *et al.*'s experiments. Some comments regarding these measurements are in order. Weinberg used a thermocouple to measure the spray water temperature. From our experience, the sheet thickness is so small and wavy that it would be difficult, if not impossible, to maintain the tip of the thermocouple in water continuously (or completely). This might explain the greater temperature rise in Weinberg's experiments. Takahashi *et al.* collected the spray water in a pool and measured the water outflow from the pool. An adiabatic screen is floated on the surface of the pool to prevent heat transfer between the steam and the subcooled pool. The adiabatic screen is suspect—especially in making measurements near the nozzle. In both the thermocouple and pool measurements, errors would result in higher temperatures than actually occurred. Their experimental values lie above the computed curve.

5. SUMMARY

Before this research was undertaken, it was believed by us (and many others) that the contraction in spray angle when a subcooled liquid was sprayed into a condensable atmosphere was primarily, if not entirely, due to drag on the droplets. That was not found to be the case. Although the sheet region may be short in length, it plays a dominant role in the contraction of the spray angle. The computed shape of the sheet region is made without any adjustable constants. The breakup length is important since it is needed to terminate the computed sheet region. Otherwise, the computed contraction would continue. An empirical expression for this breakup length as a function of Weber and Jakob numbers was obtained. The computed velocity of the liquid in the sheet at the breakup point is used as the initial velocity of the droplets. Using the measured droplet size distributions, droplet trajectories were computed. The results, which agree qualitatively with experiments, are that the small droplets are deflected inwards to a much greater extent than the larger droplets. Droplets greater than 100 μm (a large percentage of the droplets) follow a nearly straight trajectory. Finally, for the tests conducted, the fluid flow in the sheet region is laminar and thus these results are limited to laminar flow.

Acknowledgements—The authors wish to thank Professors Bankoff and Yuen for their helpful suggestions. The U.S. Nuclear Regulatory Commission, under Contract NRC-G-04-8L-020 provided financial support for this study.

REFERENCES

1. S. Y. Lee and R. S. Tankin, Study of liquid spray (water) in a non-condensable environment (air), *Int. J. Heat Mass Transfer* **27**, 351–361 (1984).
2. G. Brown, Ph.D. thesis, Imperial College of Science and Technology, London (1948).
3. G. Brown, Heat transmission by condensation of steam on a spray of water drops, *Proc. General Discussion on Heat Transfer*, Inst. Mech. Engrs (1951).
4. I. S. Lim, S. G. Bankoff, R. S. Tankin and M. C. Yuen, Cocurrent steam/water flow in a horizontal channel, NUREG/CR-2289 (1981).
5. D. Hasson, D. Luss and R. Peck, Theoretical analysis of vapor condensation on laminar liquid jets, *Int. J. Heat Mass Transfer* **7**, 969–981 (1964).
6. D. Hasson, D. Luss and U. Navon, An experimental study of steam condensation on a laminar water sheet, *Int. J. Heat Mass Transfer* **7**, 983–1001 (1964).
7. S. S. Kutateladze, Heat transfer by condensation and boiling (1952), cited by the same author in *Concise Encyclopedia of Heat Transfer*. Pergamon Press, Oxford (1966).
8. S. Weinberg, Heat transfer to low pressure sprays of water in a steam atmosphere, *Proc. Inst. Mech. Engrs* **1B**, 240–258 (1952).
9. J. D. Ford and A. Lekic, Rate of growth of drops during condensation, *Int. J. Heat Mass Transfer* **16**, 61–64 (1973).
10. A. Lekic, R. Bajramovic and J. D. Ford, Droplet size distribution: an improved method for fitting experimental data, *Can. J. Chem. Engng* **54**, 399–402 (1976).
11. A. Lekic and J. D. Ford, Direct contact condensation of vapor on a spray of subcooled liquid droplets, *Int. J. Heat Mass Transfer* **23**, 1531–1537 (1980).
12. S. A. Sandoz and K. H. Sun, Modelling environmental effects on nozzle spray distribution, ASME Paper 76-WA/FE-39 (1976).
13. S. A. Sandoz and W. A. Sutherland, Core spray performance, experimental and analytical model of LWR safety experiments, presented at the 19th National Heat Transfer Conf., Orlando, Florida, July (1980).
14. General Electric Company, General Electric Company analytical model for loss-of-coolant analysis in accordance with 10 CFR-50 Appendix K, Amendment No. 3, effect of steam environment on BWR core spray distribution, NEDO-20566-3.
15. T. Kashiwagi and K. Oketani, Direct contact condensation on coolant fluid jets, presented at Winter Annual Meeting of ASME, November (1980).
16. K. Ohba, H. Kitada and A. Nishiguchi, Direct contact condensation of steam on a high speed spray jet of subcooled water, submitted for Int. Seminar on Nuclear Reactor Safety Heat Transfer (1980).
17. J. C. P. Huang, The breakup of axisymmetric liquid sheets, *J. Fluid Mech.* **43**(2) (1970).
18. S. A. Sandoz, Private communications, December (1981).
19. Y. Tanasawa and S. Toyoda, On the atomization of liquid jet issuing from a cylindrical nozzle, *Technology Rep. Tohoku Univ.* **19**(2) (1955).
20. K. L. DeJuhasz, Dispersion of sprays in solid-injection engines, *Trans. Am. Soc. Mech. Engrs* **53**, 65–77 (1931).
21. D. W. Lee, Fuel spray formation, *Trans. Am. Soc. Mech. Engrs* **54**, 63–73 (1932).
22. F. W.-K. Chan, R. K.-C. Chan and J. H. Stuhmiller, Single nozzle spray distribution analysis, EPRI Report, NP-1344 (1980).
23. Y. Takahashi, M. Masuda, K. Aikawa and M. Tahara, A basic study of mixture-type steam condensers, Mitsubishi Heavy Industries Technical Report, Vol. 9, No. 1 (1972).

ETUDE D'UNE PULVERISATION DE LIQUIDE (EAU) DANS UN ENVIRONNEMENT CONDENSABLE (VAPEUR D'EAU)

Résumé—On propose un modèle pour décrire le comportement d'une pulvérisation d'eau froide dans un environnement de vapeur d'eau. La chute de pression dans la portion du contour est due à la condensation. Cette chute de pression est suffisante pour provoquer la contraction du contour et pour réduire l'angle d'expansion. Des résultats de calculs sont comparés aux expériences et l'accord est raisonnable. Dans ces expériences, l'écoulement du fluide dans la portion de l'enveloppe, basé sur le nombre de Reynolds, est laminaire. On suppose aussi dans les calculs que les valeurs de conductivité moléculaire sont utilisables pour calculer le transfert thermique dans l'eau froide. On obtient une formule donnant la longueur extrême en fonction des nombres de Weber et de Jakob.

UNTERSUCHUNG ÜBER DAS VERSPRÜHEN VON FLÜSSIGKEIT (WASSER) IN EINE KONDENSIERBARE UMGEBUNG (DAMPF)

Zusammenfassung—Es wird ein Modell vorgestellt, welches das Verhalten von im Dampf versprühtem unterkühltem Wasser beschreibt. Infolge der Kondensation tritt im Grenzflächengebiet der versprühten Flüssigkeit ein Druckabfall auf, der dazu ausreicht, die Grenzfläche einzuschnüren und so den Sprühwinkel zu verkleinern. Die berechneten Ergebnisse wurden mit experimentellen verglichen, wobei sich eine leidliche Übereinstimmung ergibt. Bei diesen Versuchen ist die Fluidströmung in der Grenzfläche, aufgrund der Reynolds-Zahl, laminar. Dies wird auch bei den Berechnungen vorausgesetzt: in dem unterkühlten Wasser wird Wärmetransport infolge molekularer Wärmeleitvorgänge angenommen. Die Lauflänge bis zur Auflösung wird mit der Weber- und der Jakob-Zahl korreliert.

ИЗУЧЕНИЕ РАСПЫЛЕНИЯ ЖИДКОСТИ (ВОДЫ) В КОНДЕНСИРУЮЩЕЙСЯ СРЕДЕ (ПАР)

Аннотация—Предложена модель, описывающая поведение переохлажденной водяной струи в паре. Перепад давления в плоской области струи обусловлен конденсацией. Этот перепад вызывает сжатие плоской области и уменьшает угол распыления. Сравнение расчетных и экспериментальных данных дает хорошее совпадение. В этих экспериментах поток жидкости в плоской области по числу Рейнольдса является ламинарным. Предположение о ламинарности использовалось также при вычислениях, поскольку при расчете теплопереноса в переохлажденной воде использовались значения молекулярной проводимости. Найдена зависимость от чисел Вебера и Якоба.